CONTACT ANALYSIS FOR RIVETED AND BOLTED JOINTS OF COMPOSITE LAMINATES

Tian-Qi Ye
Northwestern Polytechnical University
Xian, Shaanxi, 710072, P. R. China
Wei Li and Guanqing Shen
Shenyang Aircraft Research Institute

Abstract

Contact analysis for riveted and bolted joints of advanced composite laminates in aircraft structures is performed in this paper. For the investigation of the load transfer in structures, the identification of the damage zone and its mode of failure, and development of adequate bolted repair methodology of composite structures, computational strategies and numerical method, which are well suited to solve the three-dimensional contact problems for riveted and bolted joints of composite laminates, have been developed. In the analysis, the effects of gap and friction can be taken into account. An incremental technique is used and the corresponding slip and adhesion zones are found by iteratives in each load increment. In the finite element formulation, an approach to the reduction of stiffness matrix is employed, which allows to condense the unknowns on the contact boundaries and consequently to raise the efficiency of the numerical solution.

The experiments for the composite joints of various angle-ply laminates have been carried out. Good agreements can be observed by the comparison of the experimental results with the numerical ones.

Ⅰ. Introduction

The strength of joints is one of the principal technical issues facing composites incorporation into aircraft primary structure[1]. As the structural efficiency of a composite structure is established, with very few exceptions by its joints, not by its basic structure[2], the analysis of the riveted and bolted joints of composite laminates is of great significance. To understand better about mechanically fastened joints in the composite laminate structures the contact problem needs to be studied.

To the best of our knowledge the majority of works on the analysis of mechanically fastened joints were confined to two-dimensional geometrics that can be handled by analytical or empirical methods[3-5]. In order to investigate the load transfer through mechanical fasteners in composite laminate structures, to identify various modes of failure and their damage zone for a specified amount of loads applied and to develop adequate bolted repair methodology of composite structures, the computational strategy and numerical method for three-dimensional contact analysis of the riveted and bolted joints in composite laminate structure have been developed. In this analysis, the effects of gap and friction can be taken into consideration if necessary. The composite laminate consists of fiber-reinforced composite layers each with a specified fiber orientation. Each layer is modeled as a linear elastic continuum with hexagonal anisotropy about fiber orientation. 3-D isoparametric elements are used in the analysis. When friction is taken into account, the slip in the contact zone between the rivet or bolt and the composite laminates causes dissipation of energy, therefore, the whole load history has to be followed. An incremental technique is used and the corresponding slip and adhesion zones are found by the iterations in each load increment. The matrix partitioning procedure is used to condense the unknown degrees of freedom on the contact boundaries, that leads to reduce the computational efforts considerably. The experimental work has been performed. Different modes of failure can be observed in the tests. The numerical results compare favourably with the experimental ones.

Ⅱ. Basic Constitutive Relations

The composite laminate is composed of unidirectionally reinforced laminae oriented in various directions. Each lamina is modeled as a linear elastic continuum with hexagonal anisotropy about fiber orientation. With x_1 in the fiber direction, x_2 transverse to the fibers in the plane of the lamina and x_3 normal to the plane of the lamina. Because the laminae are treated as transversely isotropic materials, the number of independent elastic constants is reduced to five: $E_1, E_2, \upsilon_{12}, \upsilon_{23}$ and G_{12}, and the stress-strain relations can be written as

$$\begin{bmatrix}\sigma_{11}\\ \sigma_{22}\\ \sigma_{33}\\ \tau_{23}\\ \tau_{31}\\ \tau_{12}\end{bmatrix}=\begin{bmatrix}C_{11} & C_{12} & C_{12} & & & \\ C_{12} & C_{22} & C_{23} & & & \\ C_{12} & C_{23} & C_{22} & & & \\ & & & C_{44} & & \\ & & & & C_{55} & \\ & & & & & C_{55}\end{bmatrix}\begin{bmatrix}\varepsilon_{11}\\ \varepsilon_{22}\\ \varepsilon_{33}\\ \gamma_{23}\\ \gamma_{31}\\ \gamma_{12}\end{bmatrix} \tag{2.1}$$

where

$$\begin{aligned}
&C_{11}=E_1(1-\upsilon_{23}^2)/D\\
&C_{22}=E_2(1-\upsilon_{12}^2E_2/E_1)/D\\
&C_{12}=E_2(1+\upsilon_{23})\upsilon_{12}/D\\
&C_{23}=E_2(\upsilon_{23}+\upsilon_{12}^2E_2/E_1)/D\\
&C_{44}=E_2/2(1+\upsilon_{23})\\
&C_{55}=G_{12}\\
&D=1-\upsilon_{23}^2-2\upsilon_{12}^2(1+\upsilon_{23})E_2/E_1
\end{aligned} \tag{2.2}$$

Three-dimensional isoparametric hexahedron elements are used in the finite element analysis.

Ⅲ. Finite Element Formulation for Contact Analysis

Consider two elastic bodies A and B in contact along the boundary S_c shown in Figure 1. Applying the finite element method to solve the contact problem, the contacting bodies are discretized by the finite element mesh. In the analysis it is possible to find two contacting modes: node-to-node contact and node-to-surface contact. In the second case, one of the contacting point is a internal point on the surface of the solid finite element. Let k and i are a pair of contacting points on the body A and body B respectively. At the point k of body A we define a local coordinate system nst, where n is the outward normal of the body A at point k, axes s and t are located in the tangent plane. If k and i are two separate points which may contact with each other in the next increment, the axis n is fixed through the points k and i. In the node-to-surface contact case, we suppose the node k is the apex of a polyhedron, the direction of the normal n can be determined by weighted average of the normals of the surrounding planes. We take the degrees of the angles at the apex as the weighted numbers.

At the point k the displacements and tractions are denoted with

$$U_{nk}, U_{sk}, U_{tk}, T_{nk}, T_{sk}, T_{tk}$$

At the point i of the body B they are given by

$$U_{ni}, U_{si}, U_{ti}, T_{ni}, T_{si}, T_{ti}$$

In the node-to-surface contact case the displacements and tractions at the internal point of the element surface are found by the interpolation. If $\underline{U}_i$ is the vector of the displacements at internal point i, $\underline{U}_e$ is the vector of the node displacements of the element.

$$\underline{U}_i=\underline{\Phi}\,\underline{U}_e \tag{3.1}$$

where $\underline{\Phi}$ is the matrix of the interpolation functions. In accordance with the virtual work principle, one obtains

$$\underline{T}_e=\underline{\Phi}^T\underline{T}_i \tag{3.2}$$

where $\underline{T}_e$ and $\underline{T}_i$ are the vectors of the tractions at the nodes of the finite element and at the internal point respectively. In general, the normal gap may exist in the initial state or can be calculated from the previous load step, and the effect of friction has to be taken into consideration, the problem thus is solved by increments, following the loading history.

The contact conditions for the contact zones are:

on the adhesion zone,

$$\begin{aligned}
&T_{nk}+T_{ni}=0\\
&T_{tk}+T_{ti}=0\\
&T_{sk}+T_{si}=0\\
&U_{nk}-U_{ni}=U_g\\
&U_{tk}-U_{ti}=0\\
&U_{sk}-U_{si}=0
\end{aligned} \tag{3.3}$$

where the U_g stands for normal gap,

on the slip zone,

$$\begin{aligned}
&T_{nk}+T_{ni}=0\\
&T_{tk}+T_{ti}=0\\
&T_{sk}+T_{si}=0\\
&T_{tk}=T_{nk}\mu\cos\alpha\\
&T_{sk}=T_{nk}\mu\sin\alpha\\
&U_{nk}-U_{ni}=U_g
\end{aligned} \tag{3.4}$$

where μ is the friction coefficient which is assumed to be a coefficient of Coulumb friction; α is the angle of slip direction with the t-axis.

By using a incremental and iterative technique, in each increment, while iterating for correct adhesion and slip areas, the assumed adhesion and slip zones have to be verified . The verification criteria are:

for adhesion,

(1) $T_{nk}\leqslant\varepsilon$, if not satisfied, transfer to separation;

(2) $T\leqslant\mu|T_{nk}|$, if not satisfied , transfer to slip; (3.5)

where $T=T_{tk}/\cos\alpha=T_{sk}/\sin\alpha$

for slip,

(1) $T_{nk}\leqslant\varepsilon$, if not satisfied, transfer to separation;

(2) $\mathrm{sgn}(T_{tk})=-\mathrm{sgn}(U_{tk}-U_{ti})$ and $\mathrm{sgn}(T_{tk})=-\mathrm{sgn}(U_{sk}-U_{si})$, if not satisfied,

transfer to adhesion. (3.6)

Now, we discuss a condensed finite element formulation for the contact analysis.

For the body A the incremental finite element equation is written as:

$$\mathbf{K}_A\Delta\mathbf{U}_A=\mathbf{Q}_A^{(n+1)}-\mathbf{Q}_A^{(n)} \tag{3.7}$$

where $\mathbf{K}_A$ is the global stiffness matrix of the body A, $\Delta\mathbf{U}_A$ is the vector of displacement increments, $\mathbf{Q}_A^{(n+1)}$ and $\mathbf{Q}_A^{(n)}$ are the vectors of nodal forces at the step n+1 and n respectively.

Equation (3.7) can be written in the partitioned form

$$\begin{bmatrix}\mathbf{K}_{Add} & \mathbf{K}_{Adc}\\ \mathbf{K}_{Acd} & \mathbf{K}_{Acc}\end{bmatrix}\begin{bmatrix}\Delta\mathbf{U}_{Ad}\\ \Delta\mathbf{U}_{Ac}\end{bmatrix}=\begin{bmatrix}0\\ \mathbf{T}_{Ac}^{(n+1)}\end{bmatrix}+\begin{bmatrix}\mathbf{P}_{Ad}^{(n+1)}\\ 0\end{bmatrix}-\begin{bmatrix}\mathbf{F}_{Ad}^{(n)}\\ \mathbf{F}_{Ac}^{(n)}\end{bmatrix} \tag{3.8}$$

The subscript c indicates that the d. o. f. located on the contact zone.

Then, the equation (3.8) is condensed to the form

$$\Delta\mathbf{U}_{AC}=\mathbf{K}_{AC}^{-1}(\mathbf{T}_{AC}^{(n+1)}+\mathbf{Q}_{AC}) \tag{3.9}$$

where

$$\mathbf{K}_{AC}=\mathbf{K}_{ACC}-\mathbf{K}_{ACd}\mathbf{K}_{Add}^{-1}\mathbf{K}_{AdC} \tag{3.10}$$

$$\mathbf{Q}_{AC}=-\mathbf{F}_{AC}^{(n)}-\mathbf{K}_{ACd}\mathbf{K}_{Add}^{-1}(\mathbf{P}_{Ad}^{(n+1)}-\mathbf{F}_{Ad}^{(n)}) \tag{3.11}$$

Similarly we can obtain the condensed matrix of the body B:

$$\Delta\mathbf{U}_{BC}=\mathbf{K}_{BC}^{-1}(\mathbf{T}_{BC}^{(n+1)}+\mathbf{Q}_{BC}) \tag{3.12}$$

Let $\Delta\mathbf{U}$ denote the relative displacements of the contacting points

$$\Delta\mathbf{U}=\Delta\mathbf{U}_{AC}-\Delta\mathbf{U}_{BC} \tag{3.13}$$

which are involved in the contact conditions. Thus, we have

$$\begin{aligned}\Delta\mathbf{U}=&(\mathbf{K}_{AC}^{-1}\mathbf{T}_{AC}^{(n+1)}+\mathbf{K}_{BC}^{-1}\mathbf{T}_{BC}^{(n+1)})\\&+(\mathbf{K}_{AC}^{-1}\mathbf{Q}_{AC}+\mathbf{K}_{BC}^{-1}\mathbf{Q}_{BC})\end{aligned} \tag{3.14}$$

Accomplishing the coordinate transformations to the local coordinates nst defined on the contacting points, considering the contact conditions and distinguishing the unknown variables from the displacements and tractions, finally one obtains the matrix equation (3.15) for the contact analysis which is solved by the iterative technique.

$$\mathbf{u}+\mathbf{A}\mathbf{t}=\mathbf{v} \tag{3.15}$$

where $\mathbf{t}$ is a vector of contact tractions, $\mathbf{u}$ is a vector of relative displacements, the vector $\mathbf{v}$ can be determined by the substitution of the nodal forces calculated at the previous step n and the load increment.

In the computer program the condensed stiffness matrices are formed by use of the frontal method.

Ⅳ. Experiments

The strength tests have been performed for the bolted joints of composite laminates. The specimens are the single-hole bolted composite joints (Figure 2) with different angle-ply laminates (See Table 1). The major possible failure modes are: bearing failure (Figure 3(a)), tension failur(Figure 3(b)), shear-out (Figure 3(c)) and delamination (Figure 3(d)) or their combinations. The failure specimens were decomposed into individual layers and the failure modes for each layer have been investigated. For example, for a bearing failure specimen, the following failure modes were discovered:

For 0° angle-ply, the compressive failure area along the circumference of the hole is shown in Figure 4(a), it is almost symmetrical about the ordinate. For ±45° plies, the compressive failure areas are depicted in Figure 4(b) and (c), cracks can be observed in the direction perpendicular to the fiber. In the 90° ply, the crack in the matrix can be found in Figure 4(d).

Numerical analysis has been accomplished. The finite element meshes for the laminate and the bolt are shown in Figures 5 and 6 respectively. For the laminate, 3480 elements have been employed, the number of d. o. f. is 13041. For the bolt, 2520 elements and 9201 d. o. f. are used in the analysis.

The elastic constants for the composite laminates are:

$E_1=128.38\text{GPa}$, $E_2=7.9478\text{GPa}$, $G=3.5868\text{GPa}$,
$\upsilon_{12}=0.34$, $\upsilon_{23}=0.30$, the thickness of the ply $t=0.125\text{mm}$.
tensile ultimate, in fiber direction,
$\sigma_L^u=1246.6\text{MPa}$,
tensile ultimate, in the direction transverse to fiber,
$\sigma_T^u=23.128\text{MPa}$,
compressive ultimate, in fiber direction,
$\sigma_L^{cu}=841.82\text{MPa}$,
compressive ultimate, in the direction transverse to fiber,
$\sigma_T^{cu}=136.22\text{MPa}$,
ultimate shear stress,
$\tau^u=60.956\text{MPa}$.

The numerical results compare favourably with the experimental ones (see Table 2). Here the Norris failure criterion is employed.

$$\left(\frac{\sigma_{11}}{\sigma_L^u}\right)^2+\left(\frac{\sigma_{22}}{\sigma_T^u}\right)^2+\frac{\sigma_{11}\sigma_{22}}{\sigma_L^u\sigma_T^u}+\left(\frac{\sigma_{12}}{\tau^u}\right)^2=1$$

The failure zones predicted by the finite element analysis are shown in Figure 7.

Figure 8 shows the friction along the circumference of the hole, in computation it is assumed that the coefficient of friction $\mu=0.2$.

The effect of the friction on the contact pressure is shown in Figure 9. the effect of gap is shown in Figure 10.

Table 1

specimen No.	Stacking Sequence
1	0°/0°/0°/0°/90°/0°/0°/0°/0°/90°
2	±45°/90°/90°/90°/90°/90°/90°/90°/90°
3	45°/−45°/0°/0°/90°/45°/−45°/0°/0°/90°
4	45°/−45°/0°/90°/90°/45°/−45°/0°/90°/90°
5	±45°/90°/90°/90°/±45°/90°/90°/90°

Table 2

Specimen No.	Calculated Failure Stresses (MPa) (Failure Modes)	Experimental (MPa)	Error(%)
1.	421.0 (Shear, Compression)	463.0	11.2
2.	256.4 (Tension)	297.7	13.87
3.	557.3 (Bearing)	619.3	10.01
4.	486.0 (Bearing)	536.2	9.36
5.	325.9 (Bearing)	374.2	12.91

V. Conclusion

1. The computational strategy and numerical method developed in this paper are efficient for the analysis of bolted and riveted joints of composite laminates.
2. The three-dimensional contact analysis provides more accurate results for the evaluation of strength of the mechanically fastened joints in the composite structures.
3. When the joints are fastened by the bolt, the stresses normal to the laminate plane are much smaller than the normal stresses in other two directions.
4. The effect of the gap is more apparent than the effect of the friction.
5. The technique described is easily extended to multi-body contact problems, it has been implemented in the computer codes.

References

1. Wilson, Robert D., Advanced Composite Development for Large Transport Aircraft. ICAS Proc. 1988, Vol. 2. pp. 1600-1604.
2. Hart-Smith, L. J., Joints, in MATERIALS HANDBOOK, Vol. 1. Composites, pp. 479-495.
3. Godwin E. W. and Matthews, F. L., A Review of the Strength of Joints in Fibre-Reinforced Plastics. Part 1. Mechanically Fastened Joints. Composites. Vol. 11, 1980, pp. 155-166.
4. Zhang, K. D. and Veng, C. E. S., Stresses around a pin-loaded hole in orthotropic plates, J. Comp. Mat. Vol. 18. 1980, pp. 432-446.
5. Hart-Smith, L. J., Design and Analysis of Bolted and Riveted Joining Fibre-Reinforced Plastics. J. L. Matthews, Ed. Elsevier 1987. pp 227-289.
6. Chang, L. M., Numerical Method for Elasto-plastic Contact Problem and Its Application, Doctoral Thesis, Tsinghua U., 1989. (in Chinese)

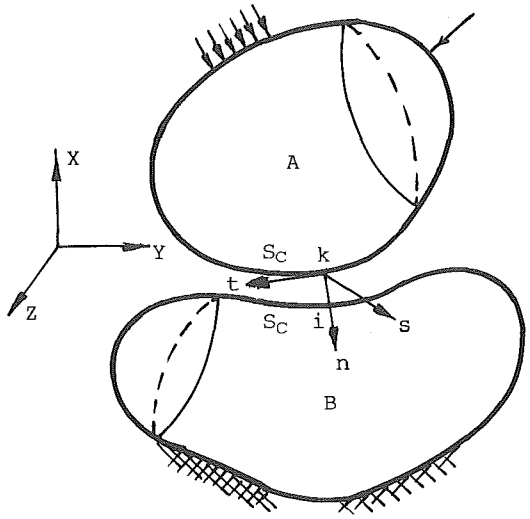

Figure 1

(a)

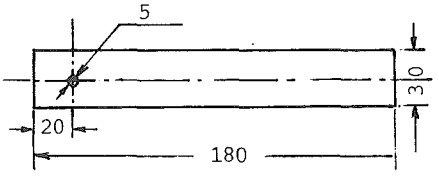

(b)

Figure 2

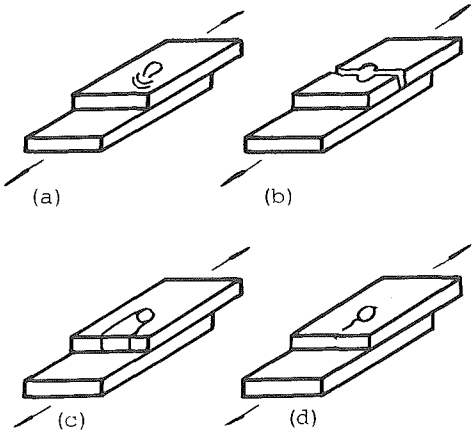

Figure 3

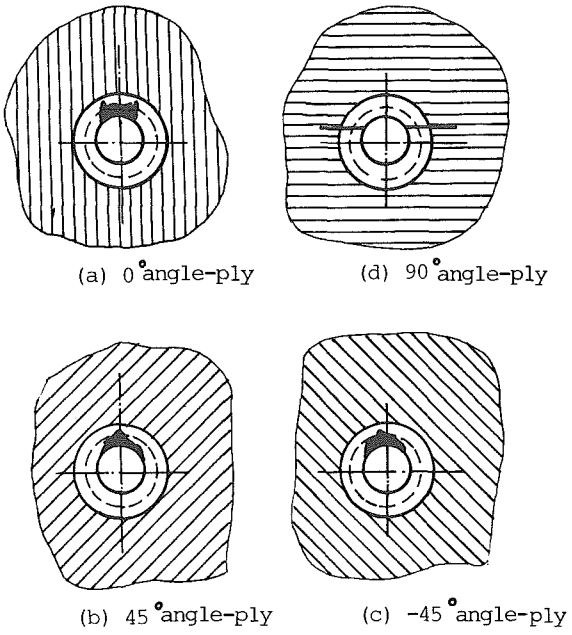

Figure 4
Fairure Modes in Testing Specimen No.4

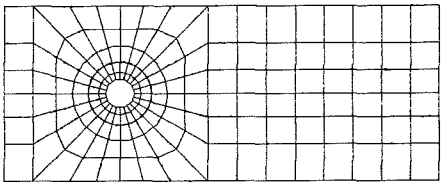

Figure 5
Composite Laminate, Mesh Subdivisions

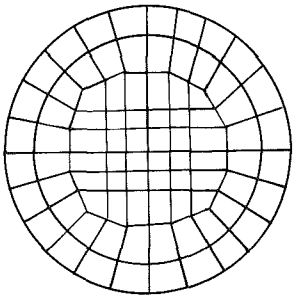

Figure 6
Bolt, Mesh Subdivisions

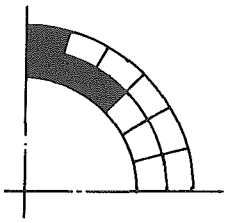

Specimen No.1

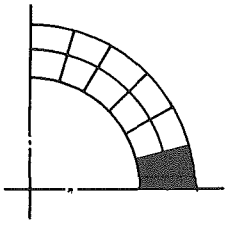

Specimen No.2

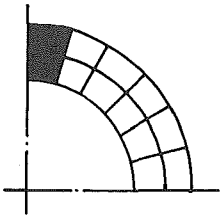

Specimen No.3

Figure 7
Failure Modes Predicted by FEM Analysis

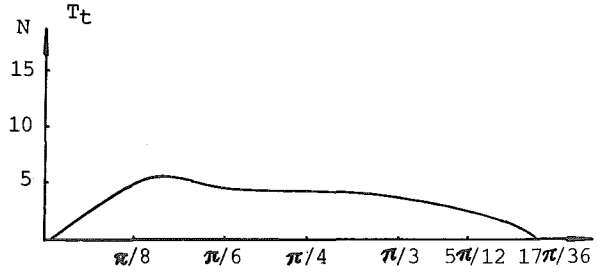

Figure 8
Distribution of Friction Force around Hole in Bottom Ply

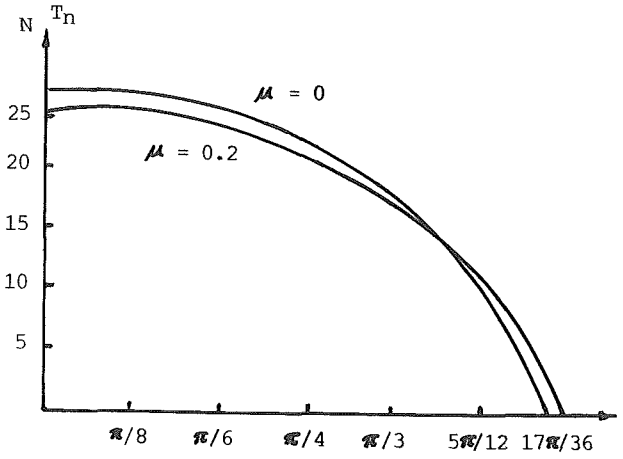

Figure 9
Distribution of Contact Force around Hole in Bottom Ply

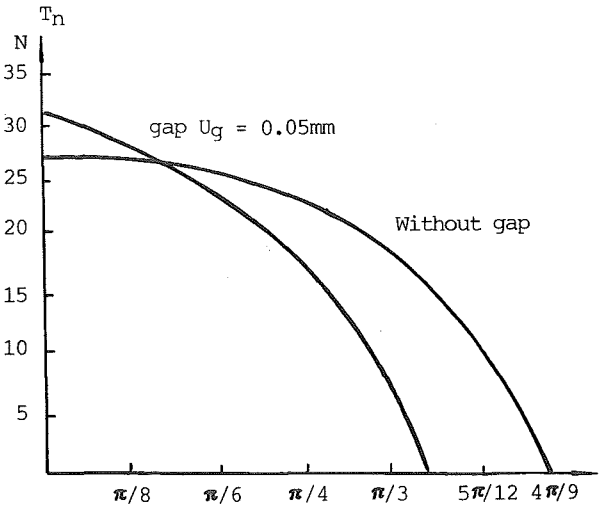

Figure 10
Distribution of Contact Force around Hole in Bottom Ply